



ELSEVIER

Analytica Chimica Acta 368 (1998) 83–89

ANALYTICA  
CHIMICA  
ACTA

## Linear calibration function for optical oxygen sensors based on quenching of ruthenium fluorescence

Han Chuang, Mark A. Arnold\*

*Department of Chemistry, University of Iowa, Iowa City, IA 52242, USA*

Received 10 June 1997; accepted 10 February 1998

### Abstract

A mathematical model is derived from the Stern–Volmer equation as a practical calibration function for various optical oxygen sensors based on quenching of ruthenium fluorescence. The model is simple and flexible, and is ideal for computing oxygen partial pressure from 0 to 760 Torr in gaseous samples, and 0 to 200 Torr in aqueous samples. Feasibility of this model for dissolved oxygen calibration is demonstrated by applying the model to data acquired from a set of three radioluminescence-based optical oxygen sensors. The model is applicable to various sensor designs and adequately accounts for stray radiation and other sources of non-quenchable light. © 1998 Elsevier Science B.V.

*Keywords:* Oxygen sensors; Optical sensors; Ruthenium fluorescence quenching; Radioluminescent oxygen sensors

### 1. Introduction

Due to their high stability, good oxygen quenchability and high quantum yield, ruthenium complexes are recognized as excellent indicators for solid-state, optical-based oxygen sensors. Operationally, these optical oxygen sensors involve immobilization of the ruthenium complex in a membrane layer, radiative excitation of the ruthenium complex, and detection of the magnitude of oxygen-induced fluorescence quenching. Various techniques have been developed for immobilizing ruthenium in a variety of membrane materials including PVC, silicon, polystyrene and sol-gel [1–10]. The resulting sensors generally show adequate stability, high selectivity, full reversibility and excellent sensitivity. Recently, the benefits of

using self-powered radioluminescent (RL) light sources have been identified for ruthenium-based oxygen sensing [11].

A major drawback in the practical application of ruthenium-based oxygen sensors is their non-linearity of response. Such sensors are based on dynamic quenching which, according to the well-known Stern–Volmer relationship, should provide a linear calibration model according to the following equation:

$$\frac{I_0}{I} = 1 + K_{SV} * [Q], \quad (1)$$

where  $I_0$  is the fluorescence intensity with absence of quencher,  $I$  is the intensity when quencher is present,  $K_{SV}$  is the Stern–Volmer constant, and  $[Q]$  is the concentration of quencher. Incorporation of the ruthenium complex in a polymer matrix results in a non-linear Stern–Volmer plot which is unfavorable for routine calibration purposes.

\*Corresponding author. Tel.: 1-319-335-1368; fax: 1-319-335-2951; e-mail: mark-arnold@uiowa.edu

Various mathematical models have been proposed [2,3,6,8,12–14] to linearize such responses. The most cited model was proposed by Carraway et al. [6]. This model is based on the concept of heterogeneous microenvironments within the polymer matrix, where different microenvironments result in different

quenching efficiencies. The following two-environment model is used most often:

$$\frac{I}{I_0} = \frac{f_1}{1 + K_{SV1} * [Q]} + \frac{f_2}{1 + K_{SV2} * [Q]}, \quad (2)$$

where  $K_{SV1}$  and  $K_{SV2}$  are the Stern–Volmer constants

Table 1  
Components for evaluated oxygen sensors

	Experiment		
	1	2	3
Membrane composition	Ru(dpp) <sub>3</sub> <sup>(a)</sup> /PVC	Ru(dpp) <sub>3</sub> /silica gel/ silicon rubber	Ru(dpp) <sub>3</sub> /TiO <sub>2</sub> /silicon rubber
RL light source	<sup>147</sup> Pm/blue phosphor	<sup>147</sup> Pm/blue phosphor	<sup>3</sup> H/blue phosphor
Wavelength selection	Monochromator	Long-pass filter	Bandpass filter
Detector	Photomultiplier tube	Silicon photodiode	Silicon photodiode
Sample	Gas	Gas	Aqueous
Sensor geometry	Planner	Planner	Tubular
Reference	[11]	[11]	[15]

<sup>a</sup>Ru(dpp)<sub>3</sub> corresponds to tris(4,7-diphenyl-1, 10-phenanthroline)ruthenium (II) chloride.

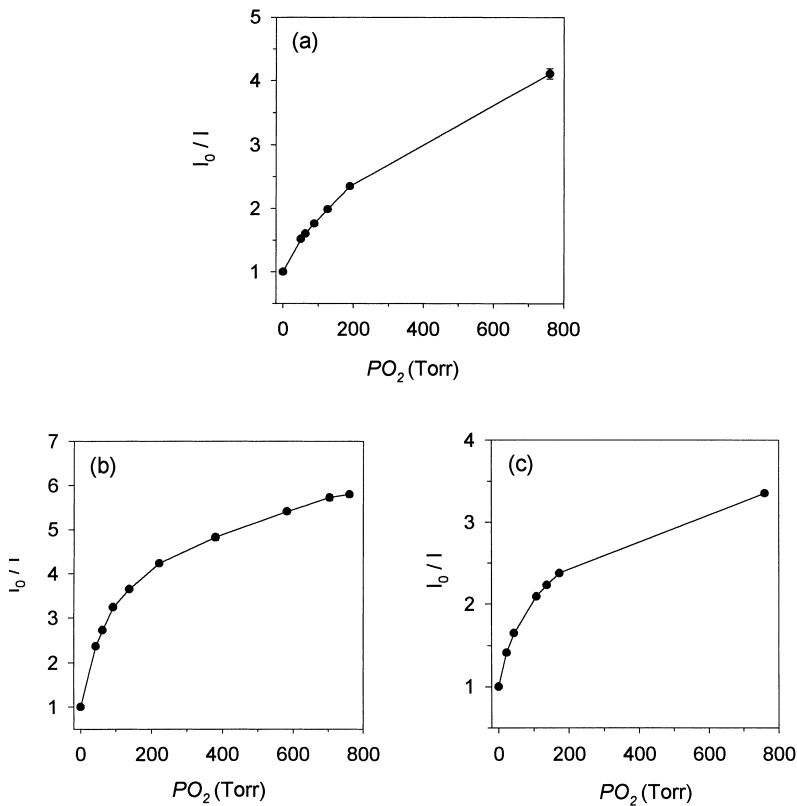


Fig. 1. Stern–Volmer plots for three optical oxygen sensors. Plots a, b and c correspond to results collected from Experiments 1, 2 and 3, respectively, list in Table 1.

for the two microenvironments, and  $f_1$  and  $f_2$  are their fractional contributions. Although multiple environments would be expected for these membrane systems [14], a simple two-component model appears sufficient to fit most calibration data.

A different model is proposed in this paper. This model is likewise based on the Stern–Volmer relationship but consider two populations of ruthenium within the membrane; one quenchable and one non-quenchable. In addition, provision is allowed to account for stray radiation within the system. The proposed model is demonstrated for a variety of ruthenium-based optical oxygen sensor designs.

## 2. Experimental

The proposed model was evaluated with data collected from three separate oxygen sensor configurations. Each uses a RL light source. Table 1

summarizes the pertinent sensor details. All three are described in more detail elsewhere, as indicated in the table. Noteworthy differences between these sensors for the purpose of testing the proposed calibration function include the membrane formulation, sensor geometry, RL source emission spectra and type of detector system.

Sensor response functions were measured by recording the fluorescence intensity as a function of time while varying oxygen levels in either a nitrogen-based gaseous stream or in water, as indicated in Table 1. Steady-state intensities were recorded for each oxygen level and used for calibration purposes.

## 3. Results and discussion

Non-linear Stern–Volmer plots are presented in Fig. 1 where Fig. 1(a), (b) and (c) correspond to

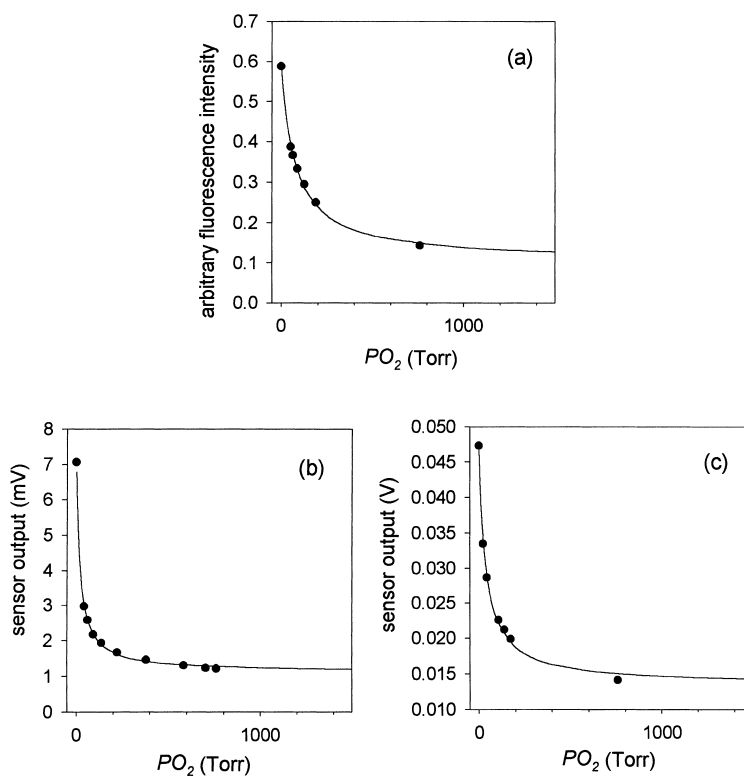


Fig. 2. Quenching plots of the three sensors. Plots a, b and c correspond to the results from Experiments 1, 2 and 3, respectively. The smooth line in each plot is the best-fitted quenching curve calculated from Eq. (4).

typical data collected in Experiments 1, 2 and 3, respectively (see Table 1). This degree of non-linearity is common for ruthenium-based oxygen probes when the ruthenium complex is immobilized in a polymer matrix. In our system, the presence of stray radiation in experiments 2 and 3 results in greater non-linearity compared to that in experiment 1. Although

the peak emission of both types of RL sources is 450 nm, each RL source emits a weak band of light around 720 nm. This second emission band is efficiently removed by the monochromator in experiment 1, but is not completely removed by the long-pass and bandpass filters used in experiments 2 and 3. This problem is exasperated by the enhanced detector

Table 2  
Regression analysis results of sensor responses

	Experiment		
	1	2	3
$K_{sv}^a$ (Torr <sup>-1</sup> )	0.0128±0.0007	0.0497±0.0016	0.0270±0.0021
Y-intercept, $I_{NQ}$	0.105±0.005 <sup>b</sup>	1.13±0.02 mV	14.0±0.4 mV
Slope, ( $I_0 - I_{NQ}$ )	0.482±0.010 <sup>b</sup>	5.93±0.05 mV	32.8±0.7 mV
$r^2$	0.9979	0.9995	0.9983

<sup>a</sup> Obtained from a nonlinear regression fit to Eq. (4).

<sup>b</sup> Arbitrary fluorescence intensity.

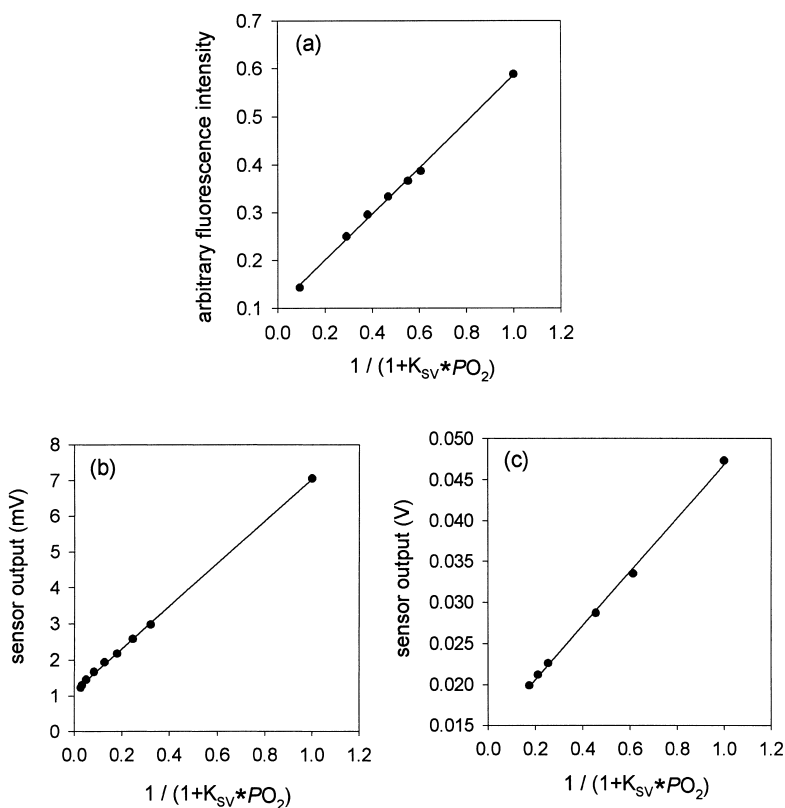


Fig. 3. Linear calibration plots for the three optical oxygen sensors using the proposed model. Lines a, b and c correspond to the results from experiments 1, 2 and 3, respectively.

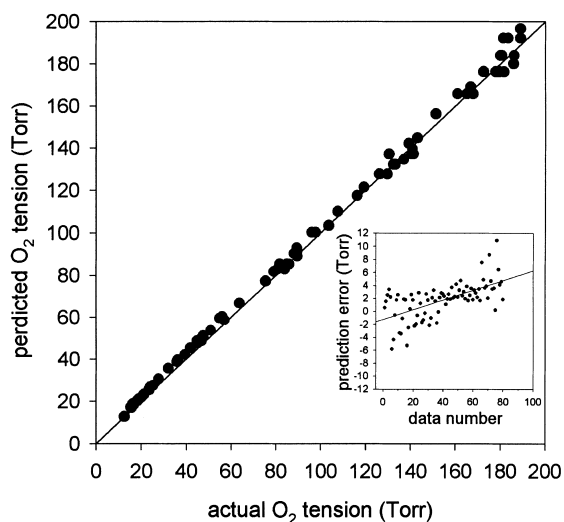


Fig. 4. Concentration correlation plot for data in Experiment 3. The inset shows tendency of the prediction error over time. The overall standard error of prediction is 3.3 Torr over a three-week experimental period.

sensitivity to these longer wavelengths. The overall effect is a significant reduction in the dynamic range and lower sensitivity at high oxygen levels.

Such oxygen sensor data can be linearized by starting with the Stern–Volmer equation and assuming the measured signal ( $I$ ) is composed of quenchable and non-quenchable radiation. The quenchable light ( $I_Q$ ) corresponds to luminescence generated from oxygen-accessible ruthenium molecules within a homogeneous membrane composition. We further assume the oxygen quenching process is uniform and adequately described by a single Stern–Volmer constant ( $K_{SV}$ ). Non-quenchable light ( $I_{NQ}$ ) corresponds to any unremoved excitation radiation, all sources of stray radiation and any non-quenchable luminescence from ruthenium aggregates within the sensing membrane. The measured intensities in the absence and presence of quencher are given as  $I_0 = I_{OQ} + I_{NQ}$  and  $I = I_Q + I_{NQ}$ , respectively. Rearranging and putting into the Stern–Volmer equation provides the following equation:

$$\frac{I_{OQ}}{I_Q} = \frac{I_0 - I_{NQ}}{I - I_{NQ}} = 1 + K_{SV} * [Q] \quad (3)$$

which can be rearranged to give the final working expression:

$$I = I_{NQ} + \frac{I_0 - I_{NQ}}{1 + K_{SV} * [Q]} \quad (4)$$

Eq. (4) indicates the measured signal ( $I$ ) is related to the quencher concentration in a complex manner. As expected, this equation shows the measured signal equals  $I_{OQ} + I_{NQ}$  in the absence of quencher and the measured signal equals  $I_{NQ}$ , when the quencher concentration approaches infinity. Fig. 2 graphically illustrates the relationship between the measured signal and oxygen concentration for each of the sensors described in Table 1 and Fig. 1. The solid lines in Fig. 2 correspond to a non-linear least squares fit of these data to Eq. (4). In each case, the fit is excellent at oxygen levels below 200 Torr with a slight positive bias at higher oxygen levels. The fitted Stern–Volmer constants are listed in Table 2 along with the corresponding fitting uncertainty.

A linear calibration plot can now be generated by using the above noted fitted Stern–Volmer constant to plot the measured signal ( $I$ ) versus  $(1 + K_{SV} * [Q])^{-1}$ . The corresponding linear plots are presented in Fig. 3 and the resulting regression coefficients are listed in Table 2 along with the computed  $r$ -square values. Again, the fits are excellent which supports the validity of the linear model.

As noted above, this calibration model works best when oxygen partial pressure ranges from 0 to 200 Torr. This range corresponds to 0–120% of air saturation for aqueous solution which is suitable for most practical applications. At elevated oxygen levels, however, significant deviations are observed between the model and actual experimental points. Such deviations are notable in Fig. 2 at 760 Torr for each of the sensors tested. Although subject to a slight positive bias, information at high oxygen levels is required during the calibration process to provide an accurate estimate of the Stern–Volmer constant.

Functional utility of the proposed linear model was demonstrated by using this model to calibrate and use the sensor described as experiment 3. In this experiment, the sensor was calibrated on day 1 and then used to measure oxygen levels in a set of aqueous samples over the next 21 days. Oxygen levels in these test samples were set randomly over a range from 0 to 180 Torr. The resulting calibration model is that presented in Fig. 3(c) with the corresponding regression coefficients listed in Table 2.

The resulting correlation plot is provided in Fig. 4 where oxygen levels predicted from the sensor response are plotted relative to the actual oxygen concentration for each of the 80 analyzed test sample. The ideal results are indicated by the unity line. Overall, model predictions follow the ideal response. The standard error of prediction and the mean percent error of prediction are 3.3 Torr and 2.8%, respectively, across the entire data set.

Closer inspection of the correlation plot reveals a slight positive bias. The Fig. 4 inset shows how the prediction error increases as a function of data number which directly relates measurement accuracy with sensor age. In fact, the magnitude of the sensor response decreases at lower oxygen levels as the sensor ages. This effect is illustrated in Fig. 5 which provides non-linear and linear response curves for days 1, 12, and 21 into this 21 day experiment.

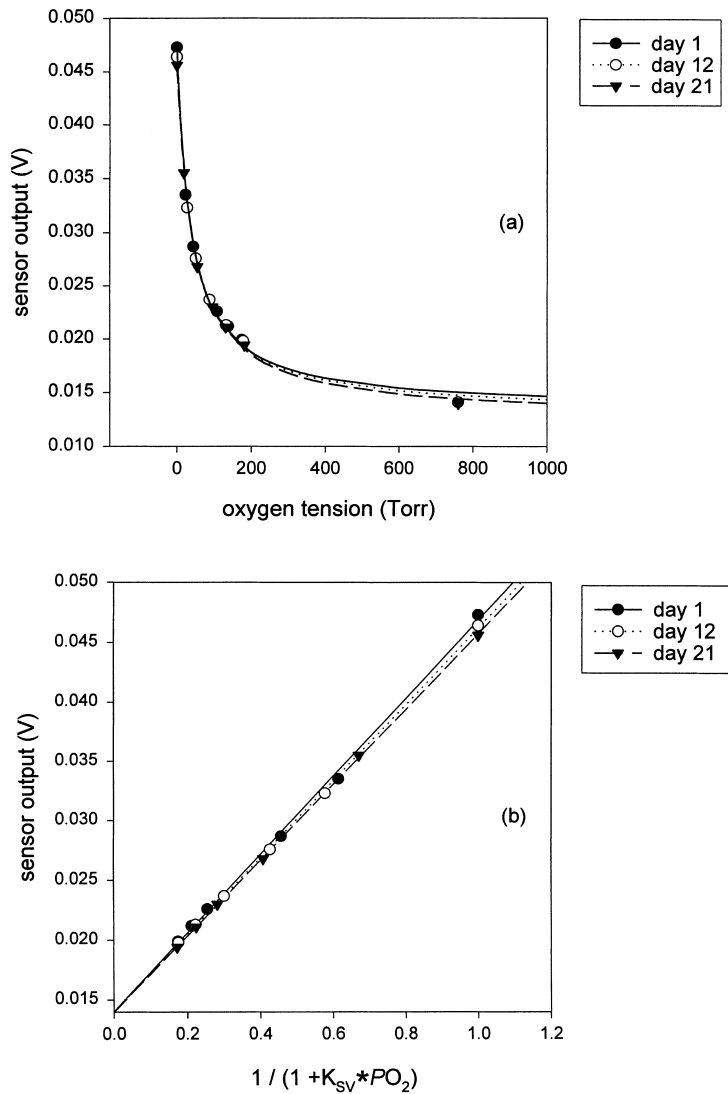


Fig. 5. Nonlinear (a) and linear (b) plots from the experiment 3 sensor for days 1 (●), 12 (○) and 21 (▼). Experimental data points and the model curves are simultaneously displayed.

Stern–Volmer constants from the non-linear plots are  $0.0270 \pm 0.0021$ ,  $0.0248 \pm 0.0015$ , and  $0.0232 \pm 0.0010 \text{ Torr}^{-1}$ , respectively. Slopes and y-intercepts from the linear plots are  $32.8 \pm 0.7$ ,  $32.2 \pm 0.7$ ,  $31.7 \pm 0.7 \text{ mV}$  and  $14.0 \pm 0.4$ ,  $14.0 \pm 0.4$ ,  $14.0 \pm 0.3 \text{ mV}$ , for days 1, 12 and 21, respectively. The consistency of the y-intercept in the linear plots indicates that the non-quenchable component of the signal is constant. This finding is supported by the similarity of signals recorded at high oxygen levels (see Fig. 5(a)) where  $I_{\text{NQ}}$  is predominant. The linear plots also indicate lower slopes as the sensor ages which is consistent with a decrease in the intensity of the quenchable fluorescence in the absence of quencher. This analysis suggests that changes within the membrane layer are responsible for aging effects in the sensor response. Changes in the Stern–Volmer constant suggest physical changes within the membrane, possibly due to slow curing of the polymer matrix. Decreases in the intensity of the quenchable fluorescence suggest less “active” ruthenium in the membrane.

#### 4. Conclusions

The proposed linear model is demonstrated for our RL optical oxygen sensors based on ruthenium fluorescence quenching. The model is evaluated under a variety of experimental conditions where different sample types, RL light sources, sensor geometries, membrane compositions and detection systems are used (Table 1). Furthermore, our model should be universal in nature, thereby providing a linear calibration function for all optical oxygen sensors based on ruthenium luminescence. When compared to other well-accepted models (such as that described in Eq. (2)) our model has the advantages of simplicity and practicability. Only two parameters,  $I_{\text{NQ}}$  and  $K_{\text{SV}}$ , are needed. However, the physical meaning associated with Eq. (2) is closer to reality because multiple

exponential decays have been observed by others based on fluorescence lifetime data [6,14]. Nevertheless, if Eq. (2) is used, care must be taken because uncounted experimental offsets (i.e., stray radiation, electronic or detector offsets, etc.) will result in misinterpretation of experimental results [15].

#### Acknowledgements

We thank Mr. P.M. Molton and R.D. Webb for their valuable information on RL sources. Support from the Microgravity Science and Applications Divisions of NASA (grant number NAG 9-824) is greatly appreciated.

#### References

- [1] C. Preininger, I. Klimant, O.S. Wolfbeis, *Anal. Chem.* 66 (1994) 1841.
- [2] M.C. Moreno-Bondi, O.S. Wolfbeis, M.J.P. Leiner, B.P.H. Schaffar, *Anal. Chem.* 62 (1990) 2377.
- [3] L. Li, D.R. Walt, *Anal. Chem.* 67 (1995) 3746.
- [4] J.R. Bacon, J.N. Demas, *Anal. Chem.* 59 (1987) 2780.
- [5] M.E. Lippitsch, J. Pusterhofer, M.J.P. Leiner, O.S. Wolfbeis, *Anal. Chim. Acta* 205 (1988) 1.
- [6] E.R. Carraway, J.N. Demas, B.A. Degraff, J.R. Bacon, *Anal. Chem.* 63 (1991) 337.
- [7] B.H. Weigl, A. Holobar, W. Trettnak, I. Klimant, H. Kraus, P. O’Leary, O.S. Wolfbeis, *J. Biotechnol.* 32 (1994) 127.
- [8] I. Klimant, O.S. Wolfbeis, *Anal. Chem.* 67 (1995) 3160.
- [9] P. Hartmann, M.J.P. Leiner, M.E. Lippitsch, *Anal. Chem.* 67 (1995) 88.
- [10] G. O’Keeffe, B.D. MacCraith, A.K. McEvoy, C.M. McDonagh, J.F. McGilp, *Sensors and Actuators B* 29 (1995) 127.
- [11] H. Chuang, M.A. Arnold, *Anal. Chem.* 69 (1997) 1899.
- [12] O.S. Wolfbeis, L.J. Weis, M.J.P. Leiner, W.E. Ziegler, *Anal. Chem.* 60 (1988) 2028.
- [13] L. Sacksteder, J.N. Demas, B.A. DeGraff, *Anal. Chem.* 65 (1993) 3480.
- [14] J.N. Demas, B.A. DeGraff, W. Xu, *Anal. Chem.* 67 (1995) 1377.
- [15] H. Chuang, Ph.D. dissertation, University of Iowa, 1997.